REPORT DOCUMENTATION PAGE

Form Approved
OMB NO. 0704-0188

1. AGENCY USE ONLY (Leave Blank)	2. REPORT DATE Feb 29, 2004	3. REPORT TYPE AND DATES COVERED Final Aug 1, 2003 - ~~Feb 1~~ 31 Jan 2004

4. TITLE AND SUBTITLE
Segmentation using Multispectral Adaptive Contours

5. FUNDING NUMBERS
~~DAAD19-03-1-0237~~
DAAD19-03-1-0237

6. AUTHOR(S)
Wesley E. Snyder

7. PERFORMING ORGANIZATION NAME(S) AND ADDRESS(ES)
North Carolina State University

8. PERFORMING ORGANIZATION REPORT NUMBER N/A

9. SPONSORING / MONITORING AGENCY NAME(S) AND ADDRESS(ES)
U. S. Army Research Office
P.O. Box 12211
Research Triangle Park, NC 27709-2211

10. SPONSORING / MONITORING AGENCY REPORT NUMBER
45753
45753.1-C1-II

11. SUPPLEMENTARY NOTES
The views, opinions and/or findings contained in this report are those of the author(s) and should not be construed as an official Department of the Army position, policy or decision, unless so designated by other documentation.

12 a. DISTRIBUTION / AVAILABILITY STATEMENT
Approved for public release; distribution unlimited.

12 b. DISTRIBUTION CODE

13. ABSTRACT (Maximum 200 words)

Funds are requested to pursue extension of the active contour model for image segmentation to images with multispectral measurements of target and background. The popular level set approach will be compared with the older "snakes" approach both theoretically and experimentally. The several different possible ways to make use of multispectral information about targets and clutter will be analyzed and experimentally compared.

14. SUBJECT TERMS			15. NUMBER OF PAGES 49
			16. PRICE CODE
17. SECURITY CLASSIFICATION OR REPORT UNCLASSIFIED	18. SECURITY CLASSIFICATION ON THIS PAGE UNCLASSIFIED	19. SECURITY CLASSIFICATION OF ABSTRACT UNCLASSIFIED	20. LIMITATION OF ABSTRACT UL

Segmentation using Multispectral Adaptive Contours

Final Report

To U.S. Army Research Office

On contract #DAAD-19-03-1-0237

Submitted by Wesley Snyder, Ph.D.

Department of Electrical and Computer Engineering

North Carolina State University

February 29th, 2004.

Table of Contents

List of all participating personnel earned advanced degrees while employed on the project

Cheolha Pedro Lee, PhD student supported on this project, anticipated graduation, Dec. 2004.

Segmentation using Multispectral Adaptive Contours

Introduction

Vector-valued images provide data in a form of vector-pixels. Multi or hyperspectral images are particular cases of vector-valued images, which consist of a stack of two-dimensional images, each measured at different wavelength band. A simple case of multispectral images is a color image, consisting of red, green, and blue (RGB) channels. Hyperspectral images are another example, which often contain more than hundred bands. Multispectral images have been studied mainly in target detection and remote sensing scenarios.

Active contours have been used for image segmentation since the first introduction of *snakes* by Kass *et al*. [11]. The basic idea is to evolve a contour *C*, subject to constraints from a given image *I*, in order to detect objects in the image. For instance, starting with a contour around the object to be detected, the contour moves towards its normal and has to stop on the boundary of the object. The evolution of the contour is obtained by minimizing an energy function with respect to *C*, and the minimizer is given by the boundary of the object. The classical approaches use the image gradient to locate the boundary of the object. In the problems of contour evolution, the level set method and the motion by mean curvature of Osher and Sethian [18] have been used extensively, because they allow for automatic topological changes. Moreover, the discretization of the problem is made on a fixed rectangular grid. Active contours provide segments in a form of closed curves (continuous boundaries), while local filtering based edge detectors, i.e. Canny [1] or Sobel operators, often provide discontinuous boundaries. However, active contours have a few disadvantages; (a) Active contours may converge to a local minimum instead of the global minimum if the initial contour is placed at an improper position. This problem makes it difficult to apply active contours in a complex image, particularly a textured image. This problem also increases the impact of noise. (b) The computational cost is higher than other segmentation methods. Since multispectral image processing has the same drawback, the application of active contours on vector-valued images is a difficult task.

The intent of this research is to investigate the performance of active contours as an image segmentation tool for vector-valued images, particularly multispectral images. A review of published methods has been performed, along with numerical experiments. In this report, we divided active contours into two

groups; (a) geometry- or boundary-based models and (b) statistics- or region-based models. Boundary-based active contour models use the image gradient to stop the evolution of contours on the desired boundary. Two boundary-based active contour models are reviewed in this report; geometric active contours proposed by Caselles *et al*. [2] and by Malladi and Sethian [13, 14] and geodesic active contours proposed by Caselles *et al*. [3, 4, 22, 23]. Region-based active contour models use stochastic information of segments to stop the contour evolution on the desired boundary. Two region-based active contour models are reviewed in this report; one proposed by Chan and Vese [5, 6, 7, 8] and the other proposed by Rousson and Deriche [21].

Most active contour models applicable to vector-valued images [7, 22, 23, 25] evolve the contour based on the sum of energy terms calculated in each frame. Since hyperspectral images may have up to hundreds of bands, this accumulation process may average out important features if they are observable only in a limited number of bands. For instance, if a set of multispectral images of a car are taken at visible bands and infrared bands, the hot spot of an engine is observed only in infrared (IR) bands. Taking the sum of energy terms along the dimension of wavelength may remove the hot spot by smoothing effect. We did an experiment of extracting a stack of *prime contours*, which are evolved from a group of frames instead of the whole frames. This new strategy divides a given hyperspectral image into a group of multispectral images with lower number of bands, based on the correlation between frames. A set of active contours – the prime contours - are evolved from each of the multispectral images. Final segmentation is achieved from these prime contours. This approach makes it possible to avoid the undesirable smoothing effect in hyperspectral image segmentation.

Contour evolution

Most active contours move towards their interior normal and stop on the boundary of the object. In most of active contours, the force to stop the contour is obtained by minimizing an energy function, and the force to move the contour is based on the mean curvature. In this section, we briefly discuss these two topics.

Energy minimization; snakes

Let a contour be normalized to have a length of one as

$$C(s):[0,1]\to\mathbb{R}^2. \tag{1}$$

The classical snake method associates the evolution of a contour C with an energy function[1] given by

$$\begin{aligned} E(C) &= \alpha\int_0^1 \left|C'(s)\right|^2 ds + \beta\int_0^1 \left|C''(s)\right|^2 ds - \lambda\int_0^1 \left|\nabla I\left(C(s)\right)\right| ds \\ &= E_{in}(C) + E_{ext}(C) \end{aligned} \tag{2}$$

where α, β, λ are real positive constants [11]. The first two terms (internal energy) control the smoothness of the curve. The first-order term with α makes the snake acts like a membrane (i.e. resists stretching), while the second-order term with β makes the snake acts like a thin plate (i.e. resists bending). The third term (external energy) with λ attracts the contour towards the boundary of the object. By minimizing this energy function, we are trying to locate the contour at the points, which maximize $|\nabla I|$, acting as an edge-detector, while keeping a smoothness in the contour.

Classical snakes have a few disadvantages; (a) they cannot detect more than one object because the contour cannot merge or break. (b) Since snakes make use of only local information, they may not find the boundary of the object if the initial position of the contour is too far from the object.

Curvature motion; level sets

Let a metric function be defined as

$$\phi(x,y,t):\mathbb{R}^2\to\mathbb{R}. \tag{3}$$

[1] This energy function is simplified particularly for the image segmentation. We are interested in closed curves (contours) only.

The contour C can be represented implicitly via this metric function by

$$C(s) \equiv \{(x, y) : \phi(x, y, t) = 0\}, \tag{4}$$

and the evolution of the contour is given by the zero-level contour at time t of the function $\phi(x,y,t)$. A common way to initiate a level set function is a signed distance to the nearest pixel on the contour. The deformation of the contour is given by

$$\begin{aligned} &\frac{\partial \phi}{\partial t} + F|\nabla \phi| = 0 \\ &\phi_0(x, y) = \pm D((x, y), C) \end{aligned} \tag{5}$$

where F is the speed function of deformation and $D(a, b)$ is the Euclidean distance between two pixels [18]. A common example of the speed function is

$$F(\kappa) = v + \varepsilon\kappa \tag{6}$$

where v is a constant speed term to accelerate the motion of a contour, and ε controls the relative importance of the curvature motion. The unit normal vector[2] and the mean curvature[3] can be directly calculated from the level set function.

$$\mathbf{n} = \frac{\nabla \phi}{|\nabla \phi|} \tag{7}$$

$$\begin{aligned} \kappa &= \operatorname{div}\left(\frac{\nabla \phi}{|\nabla \phi|}\right) \\ &= \frac{\phi_{xx}\phi_y{}^2 - 2\phi_x\phi_y\phi_{xy} + \phi_{yy}\phi_x{}^2}{\left(\phi_x{}^2 + \phi_y{}^2\right)^{3/2}} \end{aligned} \tag{8}$$

where ϕ_x and ϕ_{xx} denote the first- and second-order partial derivatives of ϕ respect to x.

The level set method has a few advantages over the classical snakes; (a) it allows for automatic topological changes, i.e. merging and breaking. (b) The discretization of the problem is made on a fixed rectangular grid. However, the computational cost is high because the dimension of the metric function to be updated is equal to the dimension of the image.

---

[2] Some literature [14, 16] defined the unit normal as $\mathbf{n} = -\nabla\phi/|\nabla\phi|$ instead of $\nabla\phi/|\nabla\phi|$ depending on the direction the normal vector towards.

[3] In the case above, curvature is defined as $\kappa = -\nabla\cdot(\nabla\phi/|\nabla\phi|)$.

Boundary (geometry) based active contours

Boundary-based active contour models use the image gradient to stop the contour evolution on the desired boundary. The stopping function can be defined as a positive and decreasing function, such as

$$g\left(I\left(x,y\right)\right)=\frac{1}{1+f\left(x,y\right)} \tag{9}$$

or

$$g\left(I\left(x,y\right)\right)=e^{-f\left(x,y\right)}, \tag{10}$$

depending on the image gradient

$$f\left(I\left(x,y\right)\right)=\left|\nabla G_{\sigma}*I\left(x,y\right)\right|^{2} \tag{11}$$

where $G_{\sigma}*I$ is a smoother version of I. The function $g(I)$ is positive in homogeneous regions, and zero at the edges

$$\begin{cases} f\to 0 & g\to 1 \\ f\to\infty & g\to 0 \end{cases}. \tag{12}$$

Geometric active contour

Caselles *et al*. [2] and Malladi *et al*. [13, 14] proposed geometric active contour models based on the mean curvature motion given by

$$\frac{\partial\phi}{\partial t}=g\left(I\right)\left(\kappa+v\right)\left|\nabla\phi\right|. \tag{13}$$

where v is a positive constant pushing the contour towards the object. The zero level contour moves in the normal direction with speed $g(I)(\kappa + v)$, and therefore stops on the desired boundary, where $g(I)$ vanishes.

Geometric active contours have a few disadvantages; (a) since the stopping function use the image gradient, boundary-based active contours make use of only local information like the classical snakes, and are sensitive to local minima and noise. (b) The initial contour should be placed at completely exterior or interior of the boundary of the object because the speed function is explicitly controlled by a constant v evolving the initial contour towards one direction.

In Figure 1, we show how geometric active contours work in a synthetic gray image. Due to the level set

implementation, the model allows automatic change of topology. In Figure 2, we show how sensitive geometric active contours are to the initial condition and noise. An initial contour is placed at the exterior of the ellipse partially overlapping the triangle. The contour cannot detect the triangle because the initial contour is not located at the complete exterior of the triangle. Due to noise, the contour cannot stop on the boundary of the object.

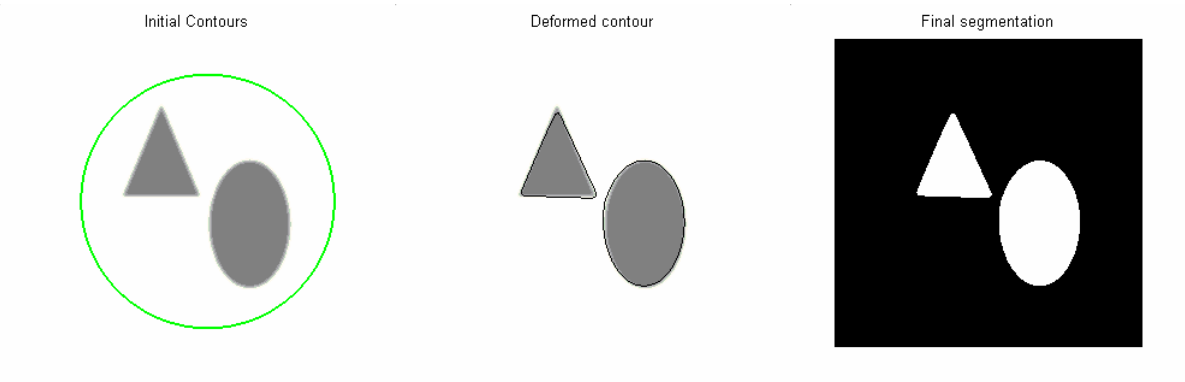

Figure 1 Geometric active contours applied into a synthetic gray image (256x256x1). (Left) An initial contour is placed at the exterior of all objects. (Middle) The contour splits and stops on the boundary of the objects. (Right) The image is divided into two segments; objects and the background.

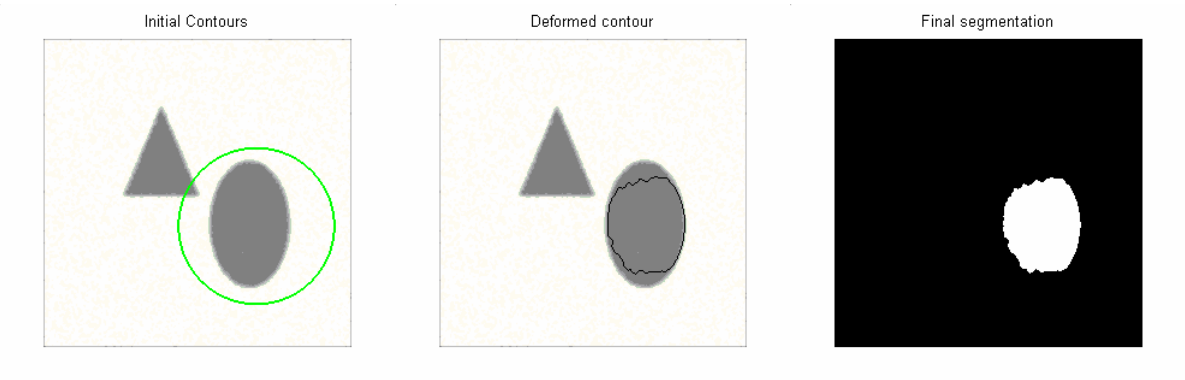

Figure 2 Geometric active contours applied into a synthetic gray image (256x256x1) corrupted by noise. (Left) Initial contour is not placed at the complete exterior of all objects. (Middle, Right) The contour cannot stop on the boundary of the object.

Let us define a vector-valued image function as

$$\mathbf{I}(x,y):\mathbb{R}^2 \to \mathbb{R}^M \tag{14}$$

with components

$$I_m(x,y):\mathbb{R}^2 \to \mathbb{R} \tag{15}$$

where m = 1, 2, …, M. An image function $\boldsymbol{I}$ at a given coordinate (x,y) is an M×1 vector. We can implement geometric active contour models into vector-valued images by using a modified version of the image gradient operator. Taking the average of the image gradient measured at each frame is an example and given by

$$f(I) = \sum_{m}^{M} w_m \left|\nabla G_\sigma * I_m\right|^2 \tag{16}$$

where w_{m} is an element of a normalized weight vector to control the relative importance of frames.

In Figure 3, three circles with different colors are placed in a synthetic RGB image (256x256x3). In Figure 4, we show how geometric active contours work on the image in Figure 3. The contour stops on the external boundary of the three circles after initilization at the exterior of the three circles. Since the segmentation relies on the deformation of a single contour, we cannot find more than two segments simultaneously. In Figure 5, we show how we can detect the internal boundary of an object. A contour is initiated at the interior of one circle, and moves outward. The contour stops growing on the internal boundary of the circle.

Figure 3 Three circles are located in a synthetic RGB image (256x256x3). (Left) Red channel, (Middle) Green channel, (Right) Blue channel.

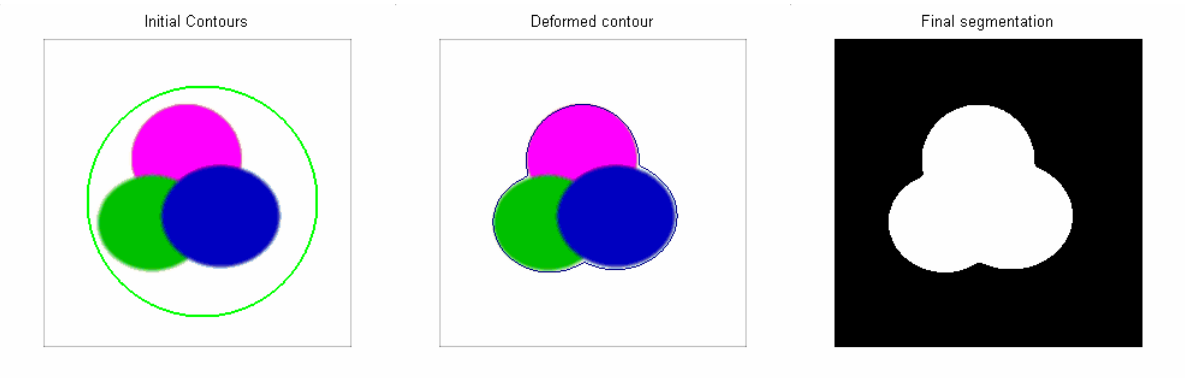

Figure 4 Geometric active contours applied into Figure 3 (256x256x3). (Left) The initial contour is placed at the exterior of three circles. (Middle) The contour stops on the external boundary of the three circles. (Right) The image is divided into two segments; three circles as one object and the background.

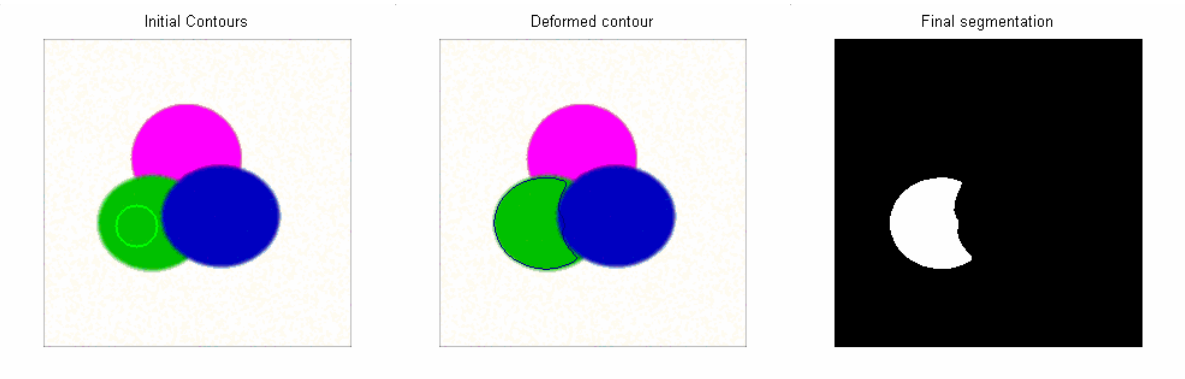

Figure 5 Geometric active contours applied into Figure 3 (256x256x3), corrupted by noise. W=[1 2 1]^T (Left) A contour is initiated at the interior of one circle. (Middle) The contour stops on the internal boundary of the object. (Right) The image is divided into two segments; a circle and the background.

In Figure 6, a toy tank is placed in a homogeneous background. In Figure 7, the same tank is placed in a textured background. Both images were measured at the inside of a room with three channels (RGB). Figure 6 represents a simple real image, while Figure 7 represents a more complicated real image with a textured background. In Figure 8, we show how geometric active contours work on the image in Figure 6. After initiating an initial contour at the exterior of the object, the contour stops at the boundary of the object providing a silhouette of the object. In Figure 9, we show how geometric active contours work on the image in Figure 7. Due to the textured background, the stopping function detects high gradient not only on the boundary of the object but also on the background. The texture of camouflage paint also

produces false edge pixels inside of the object. The contour keeps shrinking even after crossing the boundary of the object.

Figure 6 A toy tank is placed in a homogeneous background in an RGB image (258x253x3). (Left) Red channel, (Middle) Green channel, (Right) Blue channel.

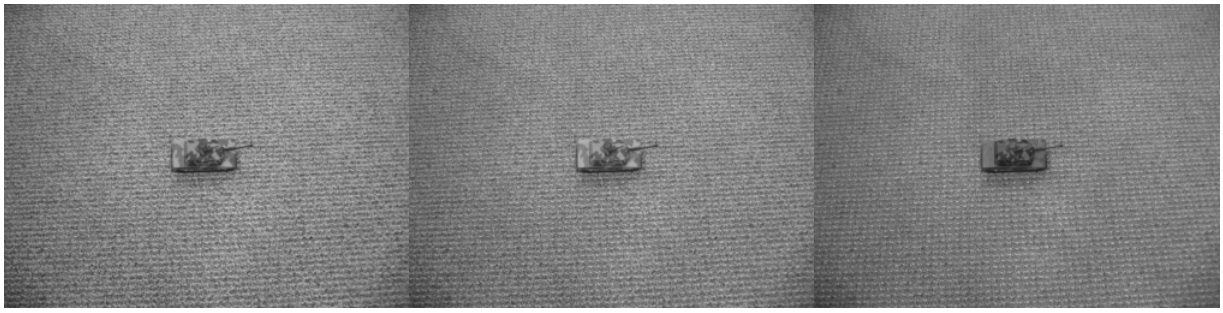

Figure 7 A toy tank is placed in a textured background in an RGB image (258x253x3). (Left) Red channel, (Middle) Green channel, (Right) Blue channel.

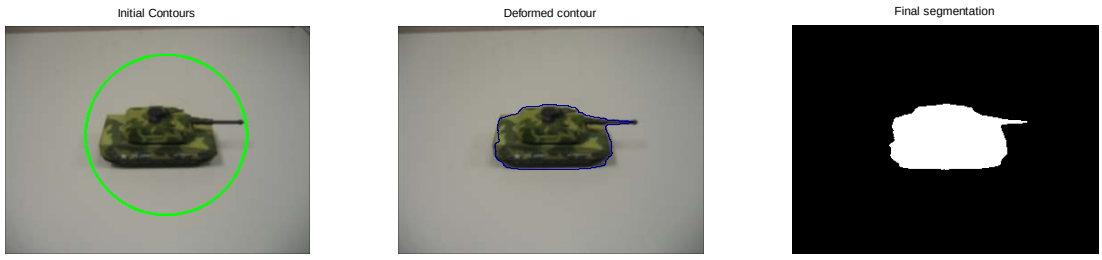

Figure 8 Geometric active contours applied into Figure 6. (Left) An initial contour is placed at the exterior of the object. (Middle) The contour stops at the boundary of the object. (Right) The image is divided into two segments; the object and the background.

Figure 9 Geometric active contours applied into Figure 7. (Left) The initial contour is placed at the exterior of the object. (Middle) (Right) The contour keeps shrinking even after crossing the boundary of the object.

Geodesic active contour

The geodesic active contour model was proposed by Caselles *et al*. in [3, 4]. They considered a particular case of the snake energy function in equation (2), where $\beta = 0$ and image gradient replaced with a decreasing gradient function

$$\begin{aligned} E(C) &= \alpha \int_0^1 \left|C'(s)\right|^2 ds + \lambda \int_0^1 g(I)\, ds \\ &= E_{in}(C) + E_{ext}(C) \end{aligned} . \tag{17}$$

Based on classical dynamical systems principles, minimizing this energy function in a certain allowed space of curves is equivalent to minimizing

$$L_R = \int_0^{L(C)} g\left(I\left(C(s)\right)\right) dv , \tag{18}$$

where *dv* is the Euclidean arc length [23]. Therefore, solving the active contour problem is equivalent to finding a path of minimal distance, where the distance is given by the modified arc length *gdv*. This path is called *geodesic curve*, and obtained by minimizing L_R. The flow minimizing L_R is given by

$$\frac{\partial C}{\partial t} = g(I)\kappa \mathbf{n} - \left(\nabla g \bullet \mathbf{n}\right)\mathbf{n} , \tag{19}$$

where κ is the mean curvature in equation (8) and **n** is the unit inward normal vector in equation (7). The complete geometric interpretation of this flow is discussed in [4, 22]. From the relation between a contour and a level set function defined in equation (4) and the level set formulation of the steepest descent method, solving this geodesic problem is equivalent to searching for the steady state of the evolution equation

$$\begin{aligned} \frac{\partial \phi}{\partial t} &= \operatorname{div}\left(g(I)\frac{\nabla \phi}{\left|\nabla \phi\right|}\right)\left|\nabla \phi\right| \\ &= g(I)\kappa\left|\nabla \phi\right| + \nabla g(I) \bullet \nabla \phi \end{aligned} . \tag{20}$$

In order to increase the convergence speed, we can add a positive constant term *v* into the evolution equation

$$\begin{aligned} \frac{\partial \phi}{\partial t} &= \operatorname{div}\left(g(I)\frac{\nabla \phi}{\left|\nabla \phi\right|}\right)\left|\nabla \phi\right| + v g(I)\left|\nabla \phi\right| \\ &= g(I)\left(\kappa + v\right)\left|\nabla \phi\right| + \nabla g(I) \bullet \nabla \phi \end{aligned} . \tag{21}$$

This is the formulation of geodesic active contour. The role of v is to increase the convergence speed by minimizing the enclosed area [9]. We can notice the geodesic active contour model is identical to the geometric active contour model in equation (13) except for $\nabla g \cdot \nabla \phi$.

In Figure 10, we show how geodesic active contours work on the same image that we used for the geometric active contours in Figure 1. As the initiated contour moves towards the boundary of objects, a set of contours automatically appear from the opposite side (inside for this case) and then move towards the boundary of objects. These dual active contours help the initiated contour not to across the weak edge pixels. The image is divided into two segments, the boundary of objects and the background.

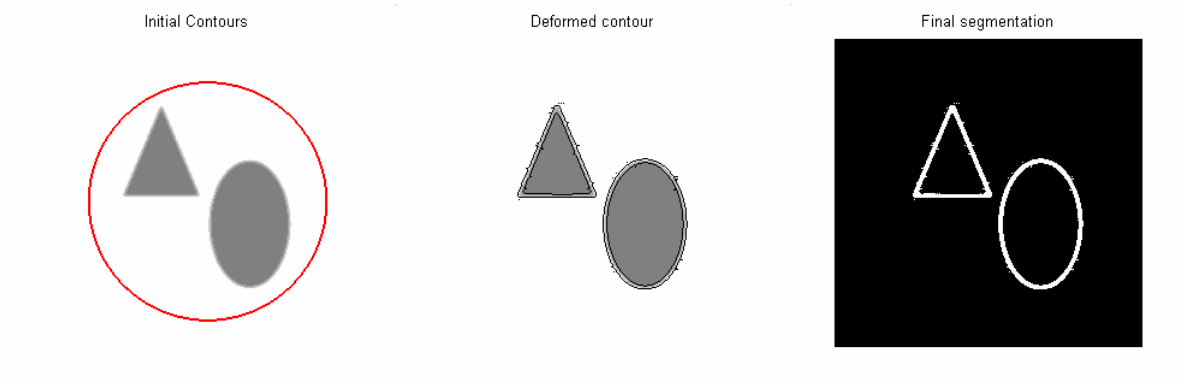

Figure 10 Geodesic active contours applied into a synthetic gray image (256x256x1). (Left) A contour is initiated at the exterior of all objects. (Middle) As the contour shrinks, a set of contours appear from the inside of objects and move towards the boundary of objects. (Right) The image is divided into two segments; the boundary of objects and the background.

Color snakes

Color snakes, a particular case of geodesic active contours on vector-valued images were proposed by Sapiro [22, 23]. He defined the edges in vector-valued images based on classical Riemannian geometry. The difference of an image function at two points P and Q is given by

$$\Delta I = I(P) - I(Q). \tag{22}$$

When the Euclidian distance between the two points $d(P, Q)$ tends to zero, the difference ΔI becomes the arc length element

$$dI = \frac{\partial I}{\partial x} dx + \frac{\partial I}{\partial y} dy. \tag{23}$$

Its squared norm is called *the first fundamental form* [12] and given by

$$dI^2 = \begin{bmatrix} dx \\ dy \end{bmatrix}^T \begin{bmatrix} g_{11} & g_{12} \\ g_{21} & g_{22} \end{bmatrix} \begin{bmatrix} dx \\ dy \end{bmatrix} \tag{24}$$

using the notation of Riemanian geometry where

$$\begin{cases} g_{12} = g_{21} = \dfrac{\partial I}{\partial x} \bullet \dfrac{\partial I}{\partial y} = \displaystyle\sum_{m=1}^{M} \dfrac{\partial I_m}{\partial x} \dfrac{\partial I_m}{\partial y} \\ g_{11} = \dfrac{\partial I}{\partial x} \bullet \dfrac{\partial I}{\partial x} = \displaystyle\sum_{m=1}^{M} \left(\dfrac{\partial I_m}{\partial x} \right)^2 \\ g_{22} = \dfrac{\partial I}{\partial y} \bullet \dfrac{\partial I}{\partial y} = \displaystyle\sum_{m=1}^{M} \left(\dfrac{\partial I_m}{\partial y} \right)^2 \end{cases} . \tag{25}$$

The extrema of this quadratic form are obtained in the directions of the eigenvectors of the metric tensor $[g_{ij}]$, and the values of the extrema are the corresponding eigenvalues given by

$$\lambda_{\pm} = \frac{g_{11} + g_{22} \pm \sqrt{\left(g_{11} - g_{22}\right)^2 + 4{g_{12}}^2}}{2} . \tag{26}$$

The eigenvector provides the direction of maximal and minimal changes at a given point in the image, and the two eigenvalues are the corresponding rates of changes, respectively λ_+ and λ_-. In single frame images, $\lambda_+ = |\nabla I|^2$ and $\lambda_- = 0$. The strength of edges in vector-valued images is a function of two eigenvalues λ_+ and λ_- rather than just the maximal rate of changes. A common choice of the edge function is

$$f\left(x, y\right) = \lambda_+ - \lambda_- = \sqrt{\left(g_{11} - g_{22}\right)^2 + 4{g_{12}}^2} . \tag{27}$$

Geodesic active contour model (21) with this particular color gradient operator constitutes the color snakes model.

In Figure 11, we show how color snakes work on the same synthetic RGB image (256x256x3), corrupted by noise this time, we used to evaluate geometric active contours in Figure 5. Compared to geometric active contours, we can notice that color snakes can detect weaker edge pixels, but are sensitive to noise.

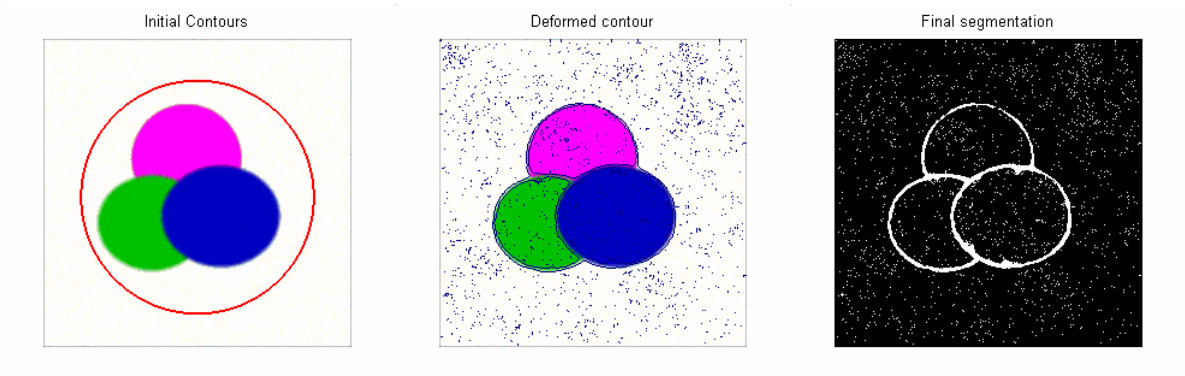

Figure 11 Color snakes applied into the RGB image in Figure 3 (256x256x3), corrupted by noise. (Left) A contour is initiated at the exterior of the three circles. (Middle) (Right) Color snakes find the boundary of three circles as well as many false segments.

In Figure 12 and Figure 13, we show how color snakes work on the same real RGB images we used to evaluate geometric active contours in Figure 8 and Figure 9. Color snakes find the many internal boundaries because of camouflage paint in both Figure 12 and Figure 13. Color snakes produces many false segments because of the textured background in Figure 13.

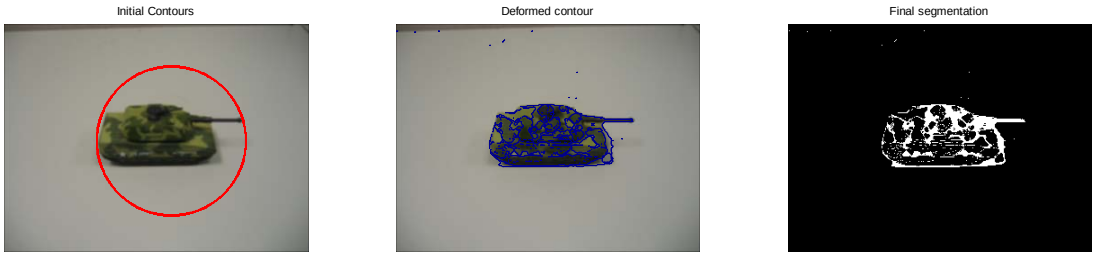

Figure 12 Color snakes applied into the RGB image in Figure 6 (258x253x3). (Left) A contour is initiated at the exterior of the object. (Middle) (Right) Color snakes find many internal boundaries because of camouflage paint.

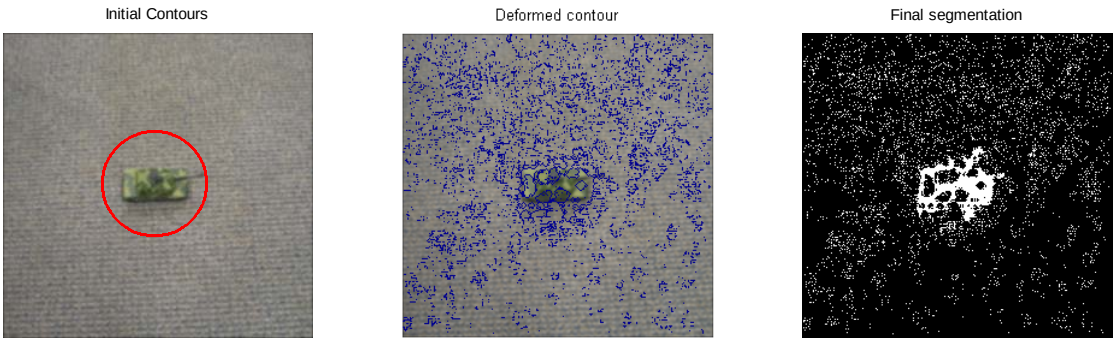

Figure 13 Color snakes applied into the RGB image in Figure 7 (258x253x3). (Left) A contour is initiated at the exterior of the object. (Middle) (Right) Color snakes produces many false segments and internal boundaries because of the textured background and camouflage paint.

Discussion

We have implemented two boundary-based active contour models; geometric active contours and geodesic active contours. Color snakes are a particular case of geodesic active contours for vector-valued images.

After numerical experiments, we found a few problems of the boundary-based active contour models. (a) Due to the structure of the speed function, boundary-based active contour models evolve the contour towards one direction. Therefore, an initial contour should be placed at completely exterior or interior of the boundary of the object. (b) Due to the image gradient operator, boundary-based active contour models may produce false segments in noisy or textured images. (c) Boundary-based active contour models cannot detect more than two segments simultaneously as they rely on single deformable contour. In Figure 4, all circles are classified into one object though each circle has different properties (color).

The sensitivity to initial condition and noise can be improved by a different approach of active contours - region-based active contour - which will be introduced in the next section. The problem of textured image can be solved by the texture based active contours, another form of active contours on vector-valued images, particularly a stack of filter responses. The problem of multiple segments can be solved by multi-phase active contours. The multi-phase active contours will be discussed after the region-based active contours in this report.

Statistics (region) based active contours

Statistics- or region-based active contour methods move contours using forces estimated from stochastic information, i.e. mean, variance, of each region instead of geometrical boundaries. An objective function is minimized by looking for the stochastic information, which characterizes the corresponding region, and the objective function acts as the stopping function without the image gradient. Two region-based active contour models, one proposed by Chan and Vese [5, 6, 7, 8, 17, 25], and the other proposed by Rousson and Deriche [17, 20, 21], will be discussed in this section.

Mumford-Shah segmentation model

Let us consider both an image as a set,

$$\Omega \subset \mathbb{R}^2 \tag{28}$$

which consists of finite number of subsets, and let a contour C be a closed subset (a contour) in Ω made up of a finite set of curves. The connected components of $\Omega \backslash C$ are defined as Ω_i, such that

$$\Omega = \left(\bigcup_i \Omega_i \right) \cup C . \tag{29}$$

We define $|C|$ as the total length of a curve C and $I_0(x,y)$ as a given image function. In [15], Mumford and Shah defined the segmentation problem as follows: find a decomposition Ω_i of Ω and an optimal piecewise smooth approximation $I(x,y)$ of the given image $I_0(x,y)$, such that $I(x,y)$ varies smoothly within each Ω_i, and discontinuously across the boundaries of Ω_i. They also proposed the following energy function[4]

$$F^{MS}(I,C) = \int_\Omega (I - I_0)^2 \, dxdy + \mu \int_{\Omega \backslash C} |\nabla I|^2 \, dxdy + \nu |C| \tag{30}$$

where μ, ν are positive constants to weight different terms in the energy. $I(x,y)$ is the minimizer of the above energy and an optimal piecewise smooth approximation of the initial, possibly noisy, image $I_0(x,y)$. C has the role of approximating the edges of $I_0(x,y)$; $I(x,y)$ will be smooth only the outside of C, i.e. $\Omega \backslash C$.

Level set method for Mumford-Shah model

Let us define the given curve C as the boundary of an open set ω

$$C = \partial\omega, \quad \omega \in \Omega , \tag{31}$$

[4] We change the notation of the given image function $I(x,y)$ in order to follow the notation in references. Note $I(x,y)$ is approximated at each iteration (time varying), while $I_0(x,y)$ is measured at only the first time (fixed). The $I_0(x,y)$ denotes the $I(x,y)$ introduced in previous sections.

and as a zero level set of a continuous function $\phi(x,y)$ [25].

$$\begin{cases} \phi(x,y) > 0 & (x,y) \in \omega \\ \phi(x,y) = 0 & (x,y) \in \partial\omega \\ \phi(x,y) < 0 & (x,y) \in \Omega \setminus \omega \end{cases} \tag{32}$$

A common way to define a level set function $\phi(x,y)$ is the signed distance to the curve C. In [10], Evans and Gariepy expressed the length of the curve C and the area of a set ω using Heaviside function

$$|C| = \int_{\Omega} |\nabla H(\phi)| \tag{33}$$

$$|\omega| = \int_{\Omega} H(\phi)\, dxdy \tag{34}$$

where Heaviside function is a unit step function given by

$$H(z) = \begin{cases} 1, & z \geq 0 \\ 0, & z < 0 \end{cases}. \tag{35}$$

Since the unit step function is not differentiable, a regularized form of Heaviside function is given by

$$H_{\varepsilon}(z) = \frac{1}{2}\left(1 + \frac{2}{\pi}\arctan\left(\frac{z}{\varepsilon}\right)\right). \tag{36}$$

The boundary of Heaviside function is a Dirac delta function approximated by

$$\delta_{\varepsilon}(z) = \frac{d}{dz} H(z) = \frac{1}{\pi} \frac{\varepsilon}{\varepsilon^2 + z^2}. \tag{37}$$

The associated Euler-Lagrange equation obtained by minimizing the length of curve in equation (33) with respect to ϕ is given by [25]

$$\begin{aligned} \frac{\partial \phi}{\partial t} &= \delta_{\varepsilon}(\phi)\, \mathrm{div}\left(\frac{\nabla \phi}{|\nabla \phi|}\right). \\ &= \delta_{\varepsilon}(\phi)\, \kappa \end{aligned} \tag{38}$$

The curve evolution motivated by the above equation can be interpreted as the motion by mean curvature minimizing the length of the curve.

Active contours without edges; Chan-Vese model[5]

A reduced case of the Mumford-Shah energy function is obtained by restricting the segmented image I(x,y) to a function, constant inside each connected component Ω_i, i.e. I(x,y) = c_i. The simplified energy function is given by

$$E^{MS}(I,C) = \sum_i \int_{\Omega_i} (I - c_i)^2 \, dxdy + v|C|. \tag{39}$$

Assuming C is fixed, the above energy is minimized by setting

$$c_i = mean(I_0(x,y)), \quad (x,y) \in \Omega_i. \tag{40}$$

Chan and Vese proposed an active contour model using this Mumford-Shah piecewise constant model [7], which does not need an edge function. They proposed to minimize the following energy function with respect to c_1, c_2, and C.

$$F_2(c_1,c_2,C) = \int_{\omega} (I_0(x,y) - c_1)^2 \, dxdy + \int_{\Omega\setminus\omega} (I_0(x,y) - c_2)^2 \, dxdy + v|C| \tag{41}$$

The above energy function can be rewritten using the level set formulation and Heaviside function as

$$\begin{aligned} F_2(c_1,c_2,\phi) = & \int_{\Omega} (I_0(x,y) - c_1)^2 \, H(\phi) \, dxdy \\ & + \int_{\Omega} (I_0(x,y) - c_2)^2 \, \{1 - H(\phi)\} \, dxdy. \\ & + v\int_{\Omega} |\nabla H(\phi)| \end{aligned} \tag{42}$$

The minimum of this energy function can be obtained by the evolution equation

$$\frac{\partial \phi}{\partial t} = \delta_{\varepsilon}(\phi)\left[v\,\mathrm{div}\left(\frac{\nabla\phi}{|\nabla\phi|}\right) - \left\{ (I_0 - c_1)^2 - (I_0 - c_2)^2 \right\} \right] \tag{43}$$

where

$$c_1 = \frac{\int_{\Omega} I_0(x,y) H_{\varepsilon}(\phi(x,y)) \, dxdy}{\int_{\Omega} H_{\varepsilon}(\phi(x,y)) \, dxdy} \tag{44}$$

[5] Although the actual title of the paper written by Chan and Vese is 'Active Contours without Edges', there are other active contour models which do not use an edge function. Thus, we will call this model as 'Chan-Vese model' following the names of the authors.

$$c_2 = \frac{\int_\Omega I_0(x,y)\left\{1 - H_\varepsilon\left(\phi(x,y)\right)\right\} dxdy}{\int_\Omega \left\{1 - H_\varepsilon\left(\phi(x,y)\right)\right\} dxdy}. \quad (45)$$

This model performs active contours looking for a 2-phase segmented image, given by

$$I(x,y) = c_1 H\left(\phi(x,y)\right) + c_2\left\{1 - H\left(\phi(x,y)\right)\right\}. \quad (46)$$

The main advantages of this active contour model compared to other active contour models are; (a) It automatically detects interior contours, so we can place a random number of initial contours in random places in the image. There are two advantages of this *distributed seed* initialization. First, we do not need prior knowledge of the possible location of the object. Second, the convergence speed increases as the number of initial contours increases. (b) Since this active contour model does not need an edge function, objects without edge lines can be detected. (c) Multiple contours can be evolved simultaneously providing multiple segments.

In Figure 14, we show how Chan-Vese model works on the same synthetic gray image (256x256x1) used to evaluate other models. 36 small initial contours were placed at random places in the image. Compared to other active contour models, Chan-Vese model is robust respect to noise.

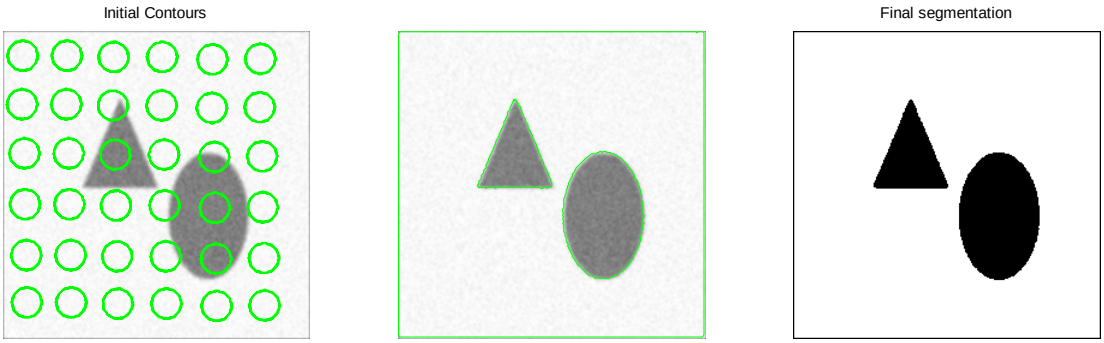

Figure 14 Chan-Vese model applied into a synthetic gray image (256x256x1) corrupted by noise. (Left) 36 small initial contours are placed using distributed seeds in the image. (Middle) (Right) The image is divided into two segments; objects and the background.

Figure 15 is a long wavelength infrared (LWIR) image measured outside. This LWIR image has low resolution and contrast. A toy truck was placed on grassland during a sunny day. The cargo bed of the truck is made of steel, while other parts of the truck are made of plastic. In Figure 16, we show the result

of Chan-Vese model applied into Figure 15. 36 initial contours are placed using distributed seeds. Active contours produce a few false segments because of the textured background.

Figure 15 An outdoor LWIR image (256x256x1) [6]. A toy truck, mainly consisting of plastic parts and metal parts, is placed on grassland.

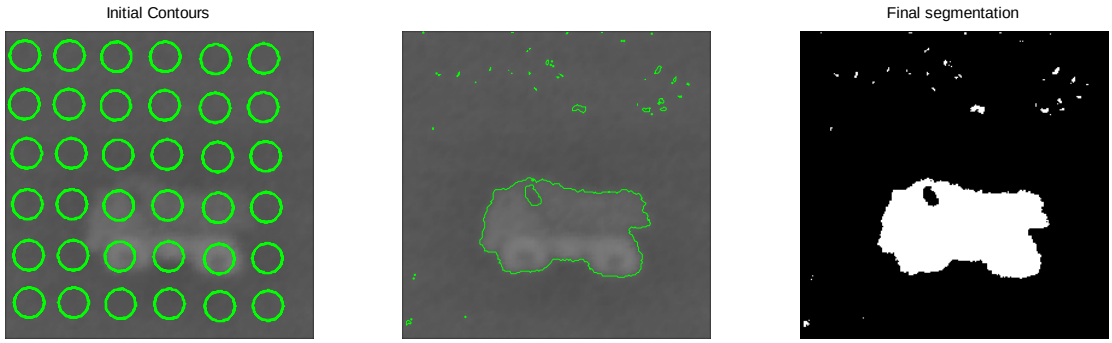

Figure 16 Chan-Vese model applied into Figure 15. (Left) 36 initial contours are placed using distributed seeds. (Middle) (Right) A few false segments are produced because of the texture of grass. The image is divided into two segments; object and the background.

In [7], Chan et al. proposed the extension of their active contour model to vector-valued images. Their model takes an average of energy functions measured at each frame. The energy function and evolution equation for vector-valued images are given by

[6] The contrast of this image is enhanced to visualize the shape of the object.

$$F_{2M}\left(\mathbf{c}_1,\mathbf{c}_2,\phi\right)=\sum_{m=1}^{M}w_{1m}\int_{\Omega}\left(I_{0m}\left(x,y\right)-c_{1m}\right)^2H\left(\phi\right)dxdy+$$
$$\sum_{m=1}^{M}w_{2m}\int_{\Omega}\left(I_{0m}\left(x,y\right)-c_{2m}\right)^2\left\{1-H\left(\phi\right)\right\}dxdy+ \quad (47)$$
$$\nu\int_{\Omega}\left|\nabla H\left(\phi\right)\right|$$

$$\frac{\partial\phi}{\partial t}=\delta_{\varepsilon}\left(\phi\right)\left[\nu\mathrm{div}\left(\frac{\nabla\phi}{\left|\nabla\phi\right|}\right)-\sum_{m=1}^{M}\left\{\left(I_{0m}-c_{1m}\right)^2-\left(I_{0m}-c_{2m}\right)^2\right\}\right] \quad (48)$$

where m = 1, 2, …, M denotes the frame of a given image. w_{1m} and w_{2m} are positive constant elements of normalized weight vectors to control the relative importance of frames. The constant functions $\mathbf{c}_1$ and $\mathbf{c}_2$ are vectors in this form.

In Figure 17, we show the result of Chan-Vese model applied into the RGB image in Figure 6 (258x253x3). 36 initial contours are placed using distributed seeds. In Figure 17, we can see more detail of the barrel of the tank than Figure 8, obtained by the geometric active contour model. In Figure 18 and Figure 19, we show the result of Chan-Vese model applied into the RGB image in Figure 7 (258x253x3). Active contours produce many false segments because of the textured background. In Figure 19, the number of false segments is reduced by placing one initial contour manually instead of distributed seeds.

Figure 17 Chan-Vese model applied into the RGB image in Figure 6 (258x253x3). (Left) 36 initial contours are placed using distributed seeds. (Middle) Active contours move towards the boundary of the object and the boundary of the image. (Right) The image is divided into two segments; the object and the background.

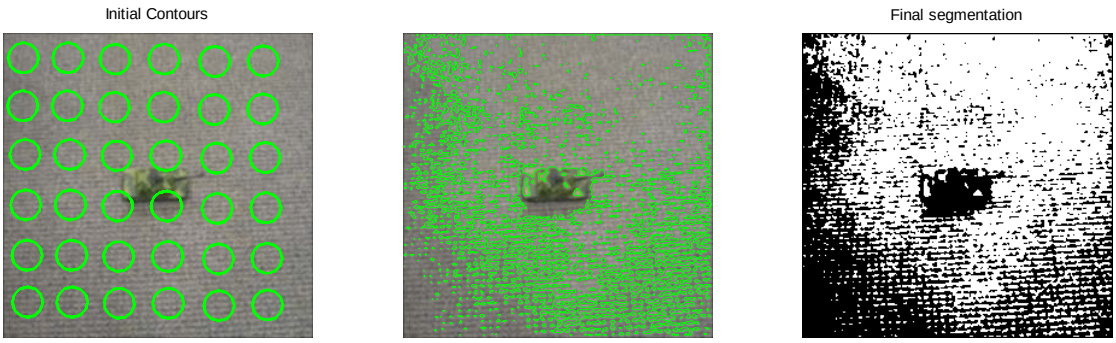

Figure 18 Chan-Vese model applied into the RGB image in Figure 7 (258x253x3). (Left) 36 initial contours are placed using distributed seeds. (Middle) (Right) Active contours produce many false segments because of the textured background.

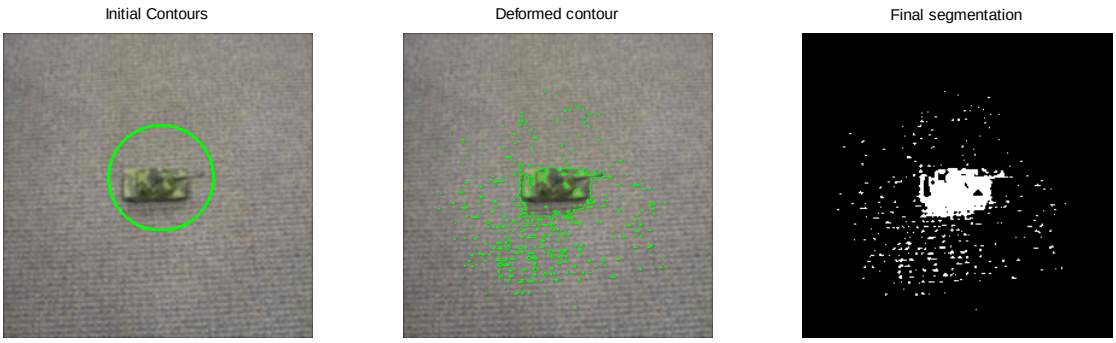

Figure 19 Chan-Vese model applied into the RGB image in Figure 7 (258x253x3). (Left) One initial contour is placed manually. (Middle) (Right) Active contours produce fewer false segments than Figure 18.

Multi-phase active contours

Multiple objects with different properties were given in Figure 4 and Figure 5, but we could detect only one object at a time because the segmentation was done by one active contour. Chan and Vese [5, 6, 17, 25], Rousson and Deriche [17, 21], and Paragios [19] proposed *multi-phase*[7] *active contour* models to detect multiple segments simultaneously. In multi-phase active contour models, we deform multiple contours simultaneously and take their combination, usually the union, to construct the final contour, which divides the image into more than two segments. The final contour can be given by

$$C = \bigcup_j C_j \tag{49}$$

where each C_j is a closed curve (contour).

Multi-phase Chan-Vese model

In [5, 6, 17, 25], Chan and Vese proposed an extension of the piecewise constant model into multi-phase segmentation. They defined $N = 2^J$ segments using J level set functions. With this definition, segments form a disjoint decomposition covering the domain Ω. There is no vacuum and overlap among segments, and we need only $\log_2 N$ level set functions to present N segments. Let us consider a vector level set function

$$\Phi(x,y) = \begin{bmatrix} \phi_1(x,y) & \phi_2(x,y) & \cdots & \phi_J(x,y) \end{bmatrix}^T \tag{50}$$

where $J = \log_2 N$ is the number of level set functions, and each level set function is defined as

$$\phi_j : \Omega \to \mathbb{R}\,. \tag{51}$$

The union of the zero level sets of ϕ_j represents the edges in the segmented image. Let us define a vector Heaviside function in the same way

$$H(\Phi) = \begin{bmatrix} H(\phi_1) & H(\phi_2) & \cdots & H(\phi_J) \end{bmatrix}^T. \tag{52}$$

Two pixels (x_1, y_1) and (x_2, y_2) belong to the same segment if and only if the corresponding Heaviside functions have the same value.

---

[7] 'Phase' is used as an equivalent term to segment. Note 'multi-phase active contours' denotes active contours with more than two phases instead of one phase. Although this definition is confusing, we followed the notation in references.

$$\left.\begin{matrix}(x_1,y_1)\\(x_2,y_2)\end{matrix}\right\}\in\Omega_i \leftrightarrow H\left(\phi(x_1,y_1)\right)=H\left(\phi(x_2,y_2)\right) \tag{53}$$

The energy function of multi-phase Mumford-Shah piecewise-constant model can be rewritten from 2-phase model in equation (41) to

$$F_N^{MS}(\mathbf{c},C)=\sum_{i=0}^{\left(N=2^J\right)-1}\left[\int_\Omega\left(I_0(x,y)-c_i\right)^2\chi_i dxdy+\frac{\nu}{2}\left|\nabla\chi_i\right|\right] \tag{54}$$

using a constant vector of averages

$$\mathbf{c}=\begin{bmatrix}c_1 & c_2 & \cdots & c_N\end{bmatrix}^T. \tag{55}$$

χ_i is the segment function denoting whether a given pixel belongs to the segment Ω_i or not. The segment functions of 2-phase model (1 level set function) are given by[8]

$$\begin{bmatrix}\chi_0\\\chi_1\end{bmatrix}=\begin{bmatrix}1-H_1\\H_1\end{bmatrix}, \tag{56}$$

and 4-phase model (2 level set functions) are given by

$$\begin{bmatrix}\chi_{00}\\\chi_{01}\\\chi_{10}\\\chi_{11}\end{bmatrix}=\begin{bmatrix}(1-H_2)(1-H_1)\\H_2(1-H_1)\\(1-H_2)H_1\\H_2H_1\end{bmatrix}. \tag{57}$$

After replacing the length of contour with the sum of the length of zero level set

$$\frac{1}{2}\sum_{i=0}^{N-1}\left|\nabla\chi_i\right|\Rightarrow\sum_{j=1}^{J}\int_\Omega\left|\nabla H_j\right|, \tag{58}$$

the energy function is given by

$$F_N^{MS}(\mathbf{c},\Phi)=\sum_{i=0}^{N-1}\int_\Omega\left(I_0(x,y)-c_i\right)\chi_i dxdy+\sum_{j=1}^{J}\nu\int_\Omega\left|\nabla H_j\right|. \tag{59}$$

For a particular example, the energy function of 4-phase model is given by

[8] Note we simplified the notation of Heaviside function. $H_j \equiv H_j(x,y) = H(\phi_j(x,y))$

$$
\begin{aligned}
F_4(\mathbf{c},\Phi) = & \int_\Omega \left(I_0(x,y)-c_{00}\right)^2 (1-H_2)(1-H_1)\,dxdy \\
& + \int_\Omega \left(I_0(x,y)-c_{01}\right)^2 (1-H_2) H_1\,dxdy \\
& + \int_\Omega \left(I_0(x,y)-c_{10}\right)^2 H_2 (1-H_1)\,dxdy \\
& + \int_\Omega \left(I_0(x,y)-c_{11}\right)^2 H_2 H_1\,dxdy \\
& + \nu\left(\int_\Omega \left|\nabla H(\phi_1)\right| + \int_\Omega \left|\nabla H(\phi_2)\right|\right)
\end{aligned} \tag{60}
$$

where $\mathbf{c} = \{c_{00}, c_{01}, c_{10}, c_{11}\}$ is a constant vector in equation (55) and $\Phi = \{\phi_1, \phi_2\}$ is a level set vector in equation (50). The segmented image function I(*x*,*y*) for 4-phase model is given by

$$
I = c_{00}(1-H_1)(1-H_2) + c_{01}(1-H_1)H_2 + c_{10}H_1(1-H_2) + c_{11}H_1H_2 . \tag{61}
$$

Two evolution equations are obtained by minimizing the above energy function as

$$
\begin{aligned}
\frac{\partial \phi_1}{\partial t} &= \delta_\varepsilon(\phi_1)\left\{\nu \mathrm{div}\left(\frac{\nabla \phi_1}{|\nabla \phi_1|}\right) - \left[\begin{array}{l}\left\{\left(I_0-c_{11}\right)^2 - \left(I_0-c_{01}\right)^2\right\} H_2 \\ + \left\{\left(I_0-c_{10}\right)^2 - \left(I_0-c_{00}\right)^2\right\}(1-H_2)\end{array}\right]\right\} \\
\frac{\partial \phi_2}{\partial t} &= \delta_\varepsilon(\phi_2)\left\{\nu \mathrm{div}\left(\frac{\nabla \phi_2}{|\nabla \phi_2|}\right) - \left[\begin{array}{l}\left\{\left(I_0-c_{11}\right)^2 - \left(I_0-c_{01}\right)^2\right\} H_1 \\ + \left\{\left(I_0-c_{10}\right)^2 - \left(I_0-c_{00}\right)^2\right\}(1-H_1)\end{array}\right]\right\}
\end{aligned} \tag{62}
$$

where the constant vector is estimated by

$$
\begin{bmatrix} c_{00} \\ c_{01} \\ c_{10} \\ c_{11} \end{bmatrix} = mean\left(I_0(x,y)\right), \quad \text{if } (x,y) \in \begin{bmatrix} \phi_2(x,y)<0, \phi_1(x,y)<0 \\ \phi_2(x,y)<0, \phi_1(x,y)>0 \\ \phi_2(x,y)>0, \phi_1(x,y)<0 \\ \phi_2(x,y)>0, \phi_1(x,y)>0 \end{bmatrix}. \tag{63}
$$

In [25], Vese proposed the extension of this model to vector-valued images as

$$
F_{NM}(\mathbf{c},\Phi) = \sum_{i=0}^{N-1}\sum_{m=1}^{M} \int_\Omega \left(I_0(x,y)-c_i\right)\chi_i\,dxdy + \sum_{j=1}^{J} \nu \int_\Omega \left|\nabla H_j\right| . \tag{64}
$$

In Figure 20 and Figure 21, we show the results of 4-phase Chan-Vese model applied into a synthetic RGB image (256x256x3) corrupted by noise in Figure 3. Four segments are defined by two level set functions. In Figure 20, two initial contours were placed manually, and the image is divided into four

segments classifying the three circles and the background separately. In Figure 21, 36x2=72 initial contours are placed using distributed seeds, and the image is divided into 3 segments misclassifying two circles as the same segment. From these experiments, we show that Chan-Vese model gives more options to place initial contours, but the segmentation result is still affected by the initial conditions.

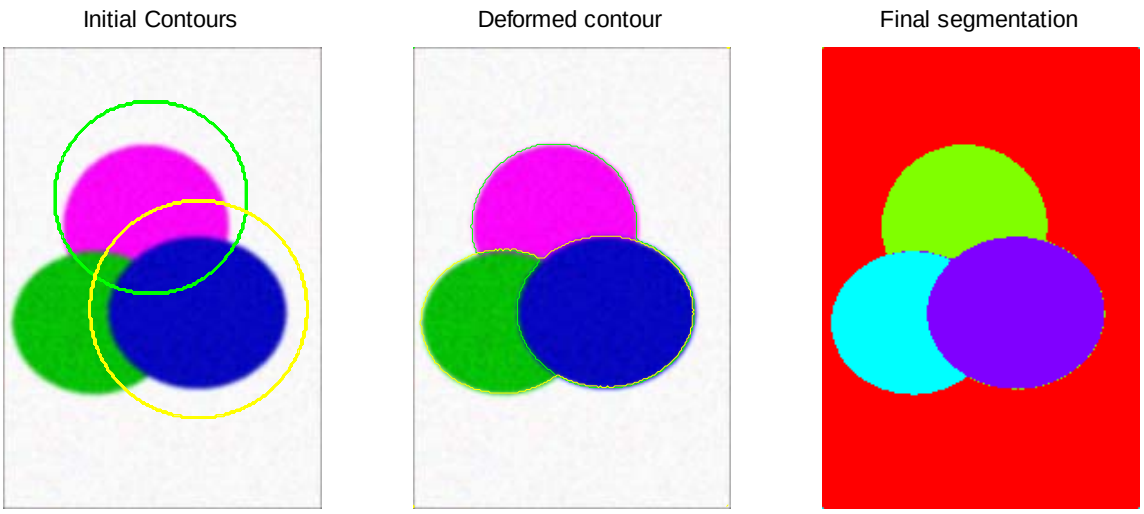

Figure 20 4-phase (2 level set functions) Chan-Vese model applied into the synthetic RGB image in Figure 3 (256x256x3), corrupted by noise. (Left) Two initial contours are placed manually. (Middle) (Right) The image is divided into 4 segments {circle 1, circle 2, circle 3, and the background}.

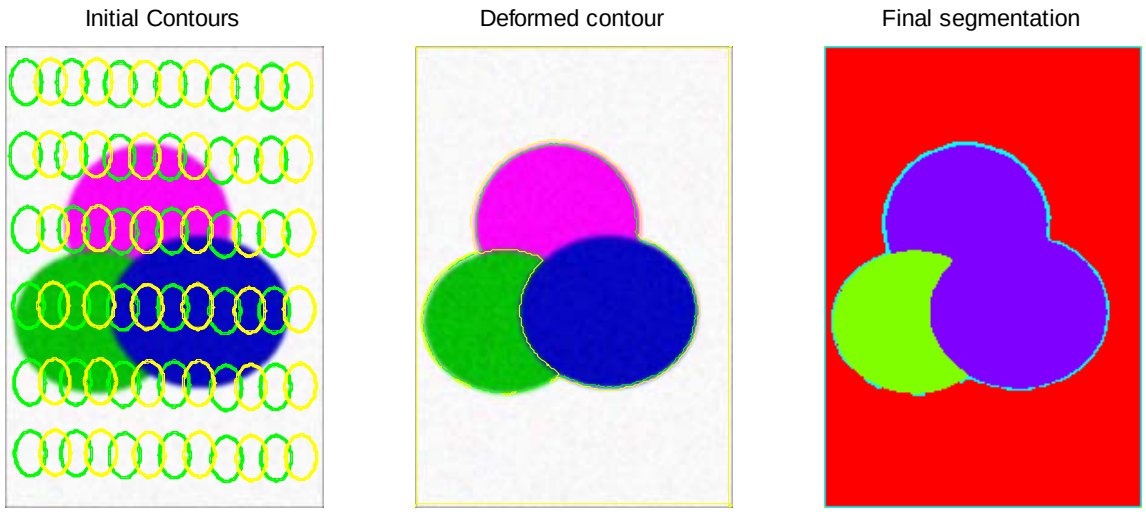

Figure 21 4-phase (2 level set functions) Chan-Vese model applied into the synthetic RGB image in Figure 3 (256x256x3), corrupted by noise. (Left) 36×2=72 initial contours are placed using distributed seeds. (Middle) (Right) The image is divided into 3 segments misclassifying two circles as the same segment.

In Figure 22, we show a real multispectral image. A toy truck was placed on the grassland during a sunny day. Seven images were measured at different wavelengths using three different sensors. The first three images were measured by an RGB camera, and the next three images were measured by an MWIR camera between 3 ~ 5 μm, and the last image was measured by an LWIR camera between 8 ~ 12 μm. The last image shows the original version of Figure 15. The segmentation of this multispectral image is a difficult task because (a) the background contains complicated texture. (b) The object consists of small sub-parts, and each subpart show different properties. The cargo part is made of yellow steel, tire part is made of black plastic, and driving seat is made of plastic with multiple colors. (c) The shadow of the object makes the spectral distribution of pixels more varied. In Figure 23, we show the result of 4-phase Chan-Vese model applied into this image set. Two sets of initial contours are placed using distributed seeds. The segmentation result is not as simple as other cases.

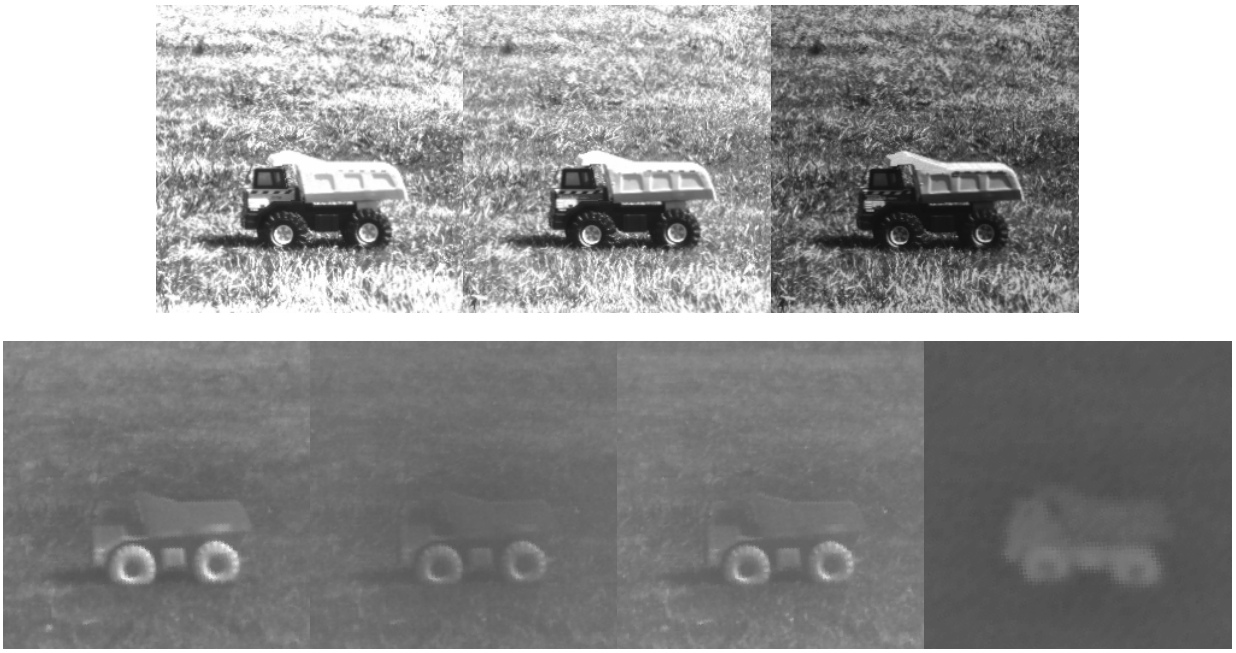

Figure 22 A 7-band multispectral image {red, green, blue, 3~5µm, 3.3~5µm, 3~4.3µm, 8~12µm} (256x256x7). A toy truck, mainly consisting of plastic parts and a few metal parts, is placed on a grass field.

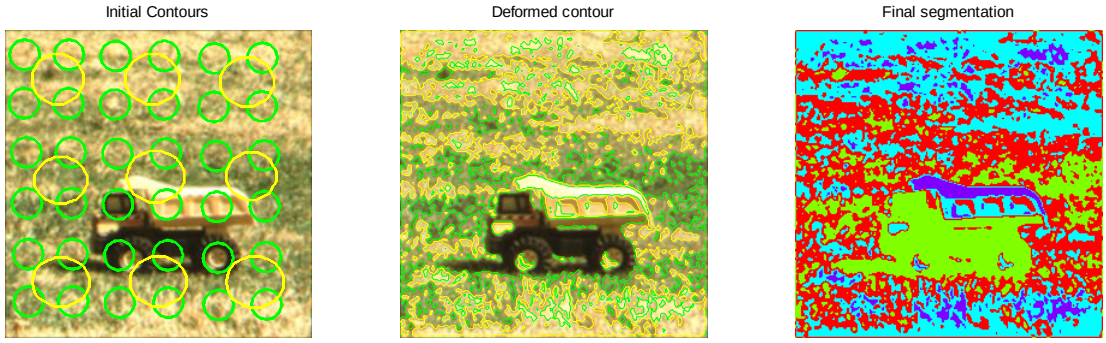

Figure 23 4-phase Chan-Vese model applied into the multispectral image in Figure 22 (7bands; 3 visible, 3 MWIR, 1 LWIR).

Multi-dimensional Gaussian fitting

In [17, 21], Rousson and Deriche proposed an active contour model using the maximization of the *a posteriori* segmentation probability. Let $p_i(I)$ be the conditional probability density function (PDF) of an image function value I with respect to the hypothesis h_i. Rousson and Deriche defined a segmentation problem as solving the optimization problem with respect to the *a posteriori* segmentation probability, given the observation set $p(\omega(\Omega)|I)$, where ω is a segment of a domain Ω. With two assumptions, (a) all segments are equally possible, (b) the pixels within each region are independent; the optimal frame segment is obtained by minimizing the following energy.

$$F(C) = \sum_{i=1}^{N} \int_{\Omega_i} -\log p_i\left(I(x,y)\right) dxdy + |C| \tag{65}$$

For a smooth non-textured image, a common choice is to use Gaussian distributions. It means that the conditional probability with respect to h_i for a vector valued image pixel $\mathbf{I}$ is

$$p_i\left(\mathbf{I}(x,y)\right) = \frac{1}{2\pi\left|\mathbf{\Sigma}_i\right|^{1/2}} e^{-\frac{1}{2}\left(\mathbf{I}(x,y)-\boldsymbol{\mu}_i\right)^T \mathbf{\Sigma}_i^{-1}\left(\mathbf{I}(x,y)-\boldsymbol{\mu}_i\right)}, \tag{66}$$

where $\boldsymbol{\mu}_i$ and $\mathbf{\Sigma}_i$ are the mean vector and covariance matrix associated to the segment Ω_i of the vector valued image $\mathbf{I}(x,y)$. Disregarding constant terms, the above energy function can be rewritten as a general form

$$F(C) = \int_{\Omega_1} e_1 dxdy + \int_{\Omega_2} e_2 dxdy + |C| \tag{67}$$

where the objective function for each segment is given by

$$e_i(x,y) = \log\left|\mathbf{\Sigma}_i\right| + \left(\mathbf{I}(x,y) - \boldsymbol{\mu}_i\right)^T \mathbf{\Sigma}_i^{-1}\left(\mathbf{I}(x,y) - \boldsymbol{\mu}_i\right). \tag{68}$$

The solution of the Euler-Lagrange equations obtained from the energy function gives expressions of $\boldsymbol{\mu}_i$ and $\mathbf{\Sigma}_i$

$$\boldsymbol{\mu}_i = \frac{\int_\Omega \mathbf{I}(x,y)\,\chi_i dxdy}{\int_\Omega \chi_i dxdy} \tag{69}$$

$$\mathbf{\Sigma}_i = \frac{\int_\Omega \left(\mathbf{I}(x,y) - \boldsymbol{\mu}_i\right)\left(\mathbf{I}(x,y) - \boldsymbol{\mu}_i\right)^T \chi_i dxdy}{\int_\Omega \chi_i dxdy} \tag{70}$$

where the segment function χ_i is identical to Chan-Vese model. The evolution equation is

$$\frac{\partial \phi}{\partial t} = \delta_{\varepsilon}(\phi)\left[v\mathrm{div}\left(\frac{\nabla \phi}{|\nabla \phi|} \right) - \{e_1 - e_2\} \right]. \tag{71}$$

This active contour model can be extended to a multi-phase model using the same set of segment functions used for Chan-Vese model.

In Figure 24 and Figure 25, we show the results of Rousson-Deriche model applied into the RGB image in Figure 7 (258x253x3). We placed an initial contour manually in Figure 24 and used distributed seeds in Figure 25. In both cases, Rousson-Deriche model find the boundary of the object in a textured background. Rousson-Deriche model is the only active contour model, which finds the boundary of the object in this image. The barrel of the tank is not detected because it is made of different material; the barrel is made of black plastic, but other parts of the tank is made of metal with camouflage paint. The image is divided into two segments; the object and the background.

Figure 24 Rousson-Deriche model applied into Figure 7 (258x253x3). (Left) An initial contour is placed manually at the exterior of the object. (Middle) The contour moves towards the object and stops on the boundary of the object. (Right) The image is divided into two sets; the object and the background.

Figure 25 Rousson-Deriche model applied into Figure 7 (258x253x3). (Left) 9 initial contours are placed using distributed seeds. (Middle) The contours move towards the object and stops on the boundary of the object. (Right) The image is divided into two sets; the object and the background.

Discussion

We have implemented two region-based active contour models: Chan-Vese active contour model based on Mumford-Shah segmentation funtion and Rousson-Deriche active contour model based on the maximization of *a posteriori* segmentation probability. After numerical experiments, these two region-based active contour models show a few advantages compared to the boundary-based active contour models; (a) region-based active contours use the global energy minimization for stopping function instead of an edge function based on the local image gradient. According to visual inspection, the global minimization often shows more reasonable segmentation result than local minimization. Not using a local edge function also gives more robustness to noise. (b) A random number of initial contours can be placed at random places in the image. Increasing the number of initial contours increases the convergence speed, and distributed seeds provide a means for an automatic segmentation tool. (c) The multi-phase segmentation makes it possible to divide an image into more than two segments.

Although the energy functions of two models to be minimized are similar, they calculate different metrics. Chan-Vese model measures a squared Euclidean distance between the given image function I and the estimated mean c_i of the corresponding region. Rousson-Deriche model measures the Mahalanobis distance, if we ignore the log term. Another difference between two models is Chan-Vese model takes the average of energy functions measured at each frame, while Rousson-Deriche model fits a multi-dimensional Gaussian distribution. Chan-Vese model can be interpreted as a particular case of Rousson-Deriche model, where the covariance matrix is fixed as an identity matrix. According to visual inspection, this multi-dimensional approach often shows more reasonable segmentation result.

Prime contours

Hyperspectral images often contain more than hundred frames. Features which discriminate particular object do not necessarily exist in all frames. For instance, a hot spot of a car engine is a discriminating feature in infrared bands, but almost invisible in visible bands. The color of flowers is a discriminating feature in visible bands, but is not a discriminating feature in infrared bands.

Most active contour models applicable to vector-valued images are extended to vector-image segmentation after being originally designed for two-dimensional image segmentation, i.e. Chan-Vese active contour model. These active contours often calculate the energy function by taking the sum of energy functions from each frame. The energy function can be high in some frames but can be low or even zero in other frames. Summing up these energies along the dimension of frames will smooth the discriminating feature, i.e. weakening the boundary of objects.

In Figure 26, we show a synthetic RGB image (256x256x3) for this kind of case. The background has intensity {180, 180, 180}. Hexagon and circle are visible in all three bands with intensity {130, 60, 90}. There are two pentagons with intensity {130, 60, 30} placed inside of the hexagon and circle. These pentagons are invisible in the red and green channels because they have the same intensity as the hexagon and circle. Information useful to extract these pentagons is available only in the blue channel. Our objective is to segment the two pentagons from the hexagon and circle. In Figure 27, we show the result of the 4-phase Chan-Vese model applied into this vector-valued image. Two pentagons are not segmented because the energy function from the blue channel is smoothed by averaging.

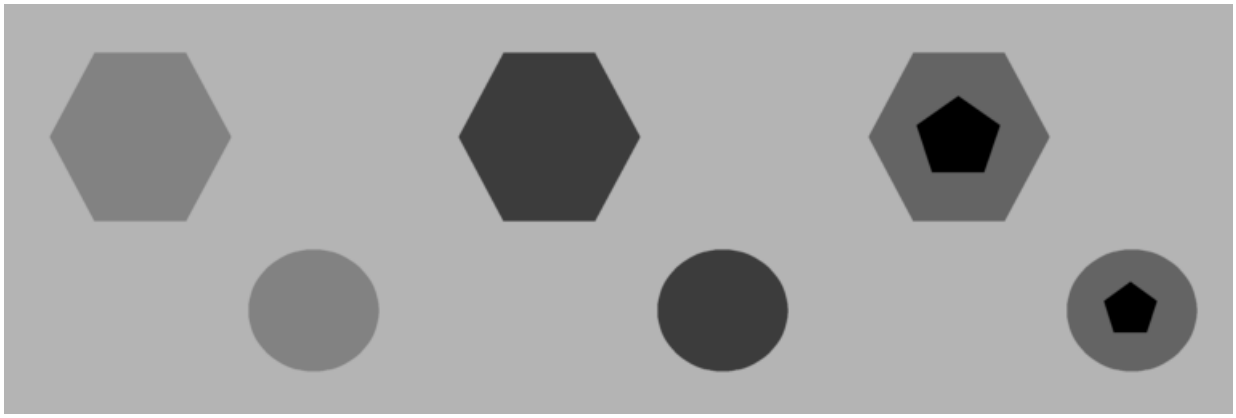

Figure 26 Four objects are placed in a synthetic RGB image (256x256x3). Only two objects, hexagon and circle, are visible in red and green channels. Two pentagons are visible inside of the hexagon and circle only in the blue channel.

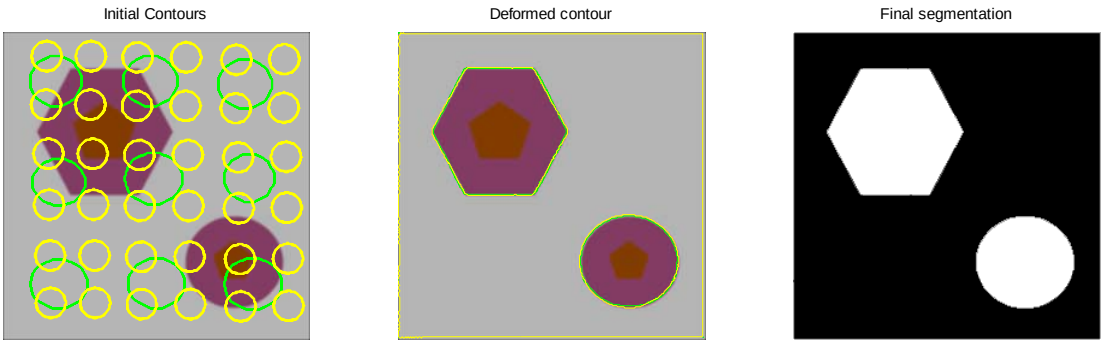

Figure 27 4-phase (2 level set functions) Chan-Vese model applied into Figure 26. (Left) Two sets of contours are initiated using distributed seeds. (Middle) Both contours cannot detect the pentagons. (Right) The image is divided into two segments only; {hexagon, circle} and background.

A pseudo multispectral image is generated from an RGB image for this experiment. The first three frames are extracted from an RGB image. The fourth frame is generated by Gaussian blurring with radius 1.0 and adding 1% uniform noise to the gray image (average of the first three channels). The fifth frame is generated by Gaussian blurring with radius 2.0 and adding 3% uniform noise to the blue channel. The sixth frame is generated by Gaussian blurring 2.0 and adding 3% uniform noise to the red channel. The seventh frame is generated by Gaussian blurring with radius 4.0 and adding 4% uniform noise to the gray image. The image pixels around the engine hood in the sixth and seventh frame are 20% lightened to make pseudo hot spot. Our objective is to segment the hot spot from the car. Figure 28 shows this pseudo multispectral image with seven bands. In Figure 29, we show the result of 2-phase Chan-Vese model applied into the image in Figure 28. The hot spot is not segmented because the averaging operation smooth energy functions from sixth and seventh frame.

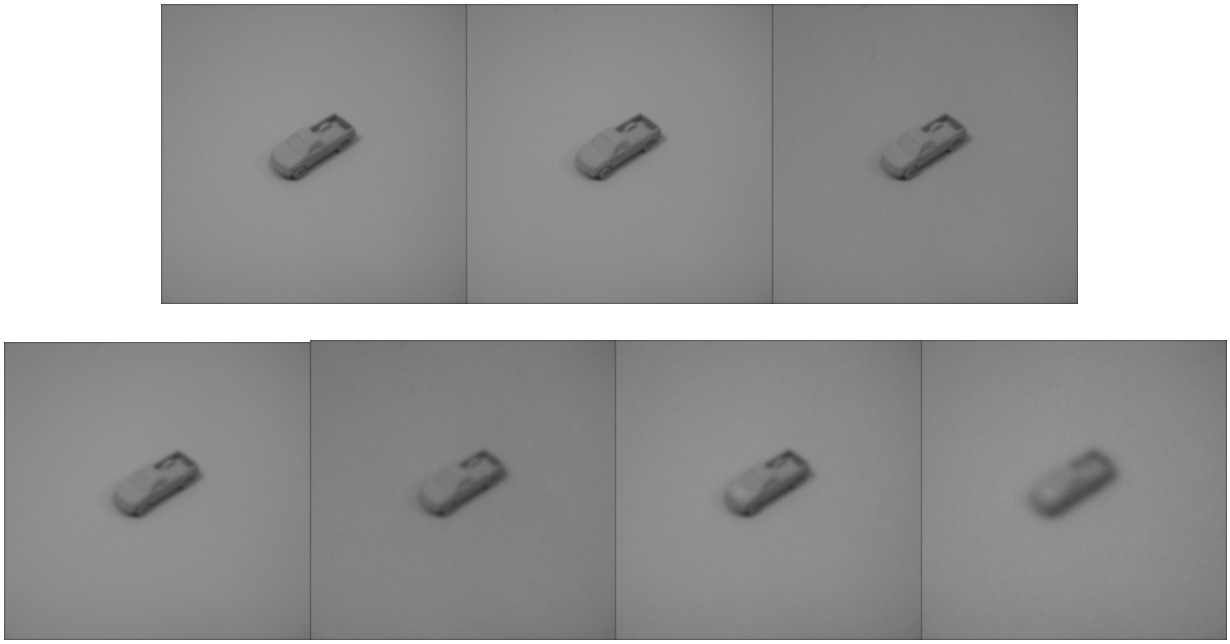

Figure 28 A pseudo multispectral image (258x253x7). (Top) The original RGB image. (Bottom) Images modified from the original RGB image.

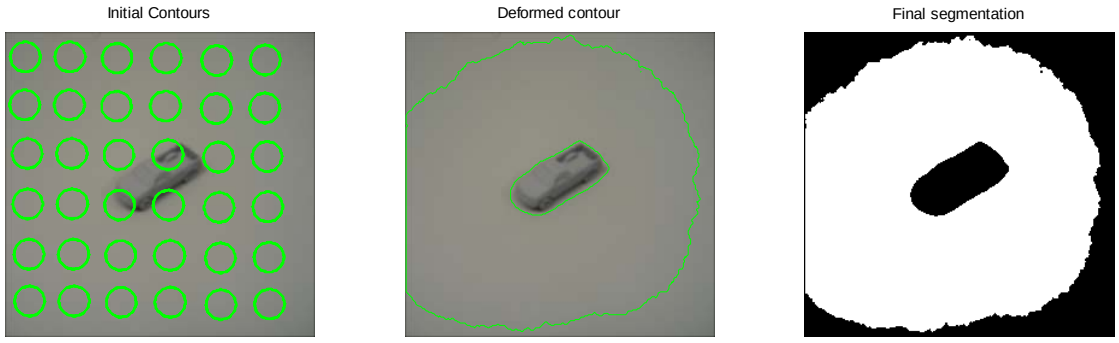

Figure 29 2-phase Chan-Vese model applied into the image in Figure 28 (7 bands). Hot spot is not segmented.

Considering the properties of hyperspectral images, if there is a discriminating feature in band A, the same discriminating feature may exist or be strong in the neighbor bands of band A. For active contours, the energy function will be kept strong enough if we take the average only within the neighbor bands instead of the whole bands. Suppose a hyperspectral image is given. We divide the given hyperspectral image into a group of multispectral images with lower number of bands, based on the correlation

between frames, i.e. {a visible band image, a SWIR band image, a MWIR band image}. A set of active contours – the prime contours - are evolved from each of the multispectral images. Final segmentation is achieved from these prime contours using the same means of multi-phase active contours. Two extreme results are possible. First, we will have an over-segmented image if the prime contours are highly uncorrelated. Second, the result will be identical to the result using other active contour models if the prime contours are completely correlated. However, most of cases will be between these two extreme results.

In Figure 30, we show the result of the proposed method applied into the same data used in Figure 27. Here, we assume that these three channels belong to different groups, so apply 4-phase Chan-Vese model separately into these three channels. The results from red and green channel are identical because they are completely correlated, but the result from blue channel show different segmentation. The final segmented image is represented by the union of three prime contours. The image is divided into three segments; {two pentagons, hexagon and circle, and background}.

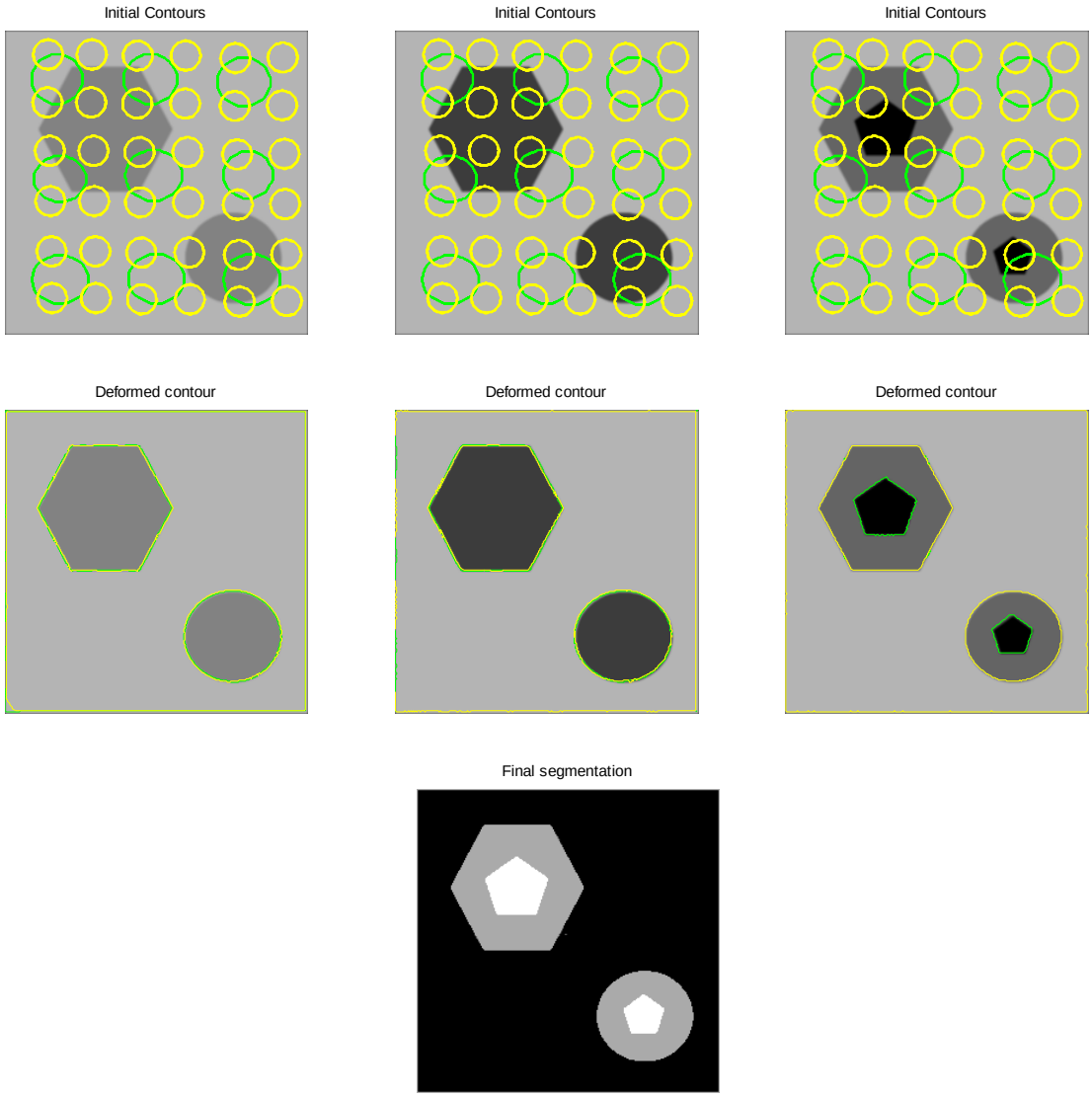

Figure 30 Proposed method applied into Figure 26 (Top) 4-phase Chan-Vese model applied separately into three channels. Initial contours are placed using distributed seeds in all three cases. (Middle) Only hexagon and circle are segmented in red and green channels, but two pentagons as well as hexagon and circle are segmented in the blue channel. (Bottom) The final result. The image is divided into three segments; {Two pentagons}, {hexagon, circle}, and the background.

In Figure 31, we show the result of proposed method applied into the image in Figure 28. First, we divide the seven frames into three groups [{1,2,3}{4,5},{6,7}]. Then, we apply 2-phase Chan-Vese model separately into these three groups. 36 initial contours are placed using distributed seeds for all

three groups. From the first two groups, active contours find only the silhouette of the car, but they find the hot spot in the third group. We represent the final segmented image by taking the union of these three images.

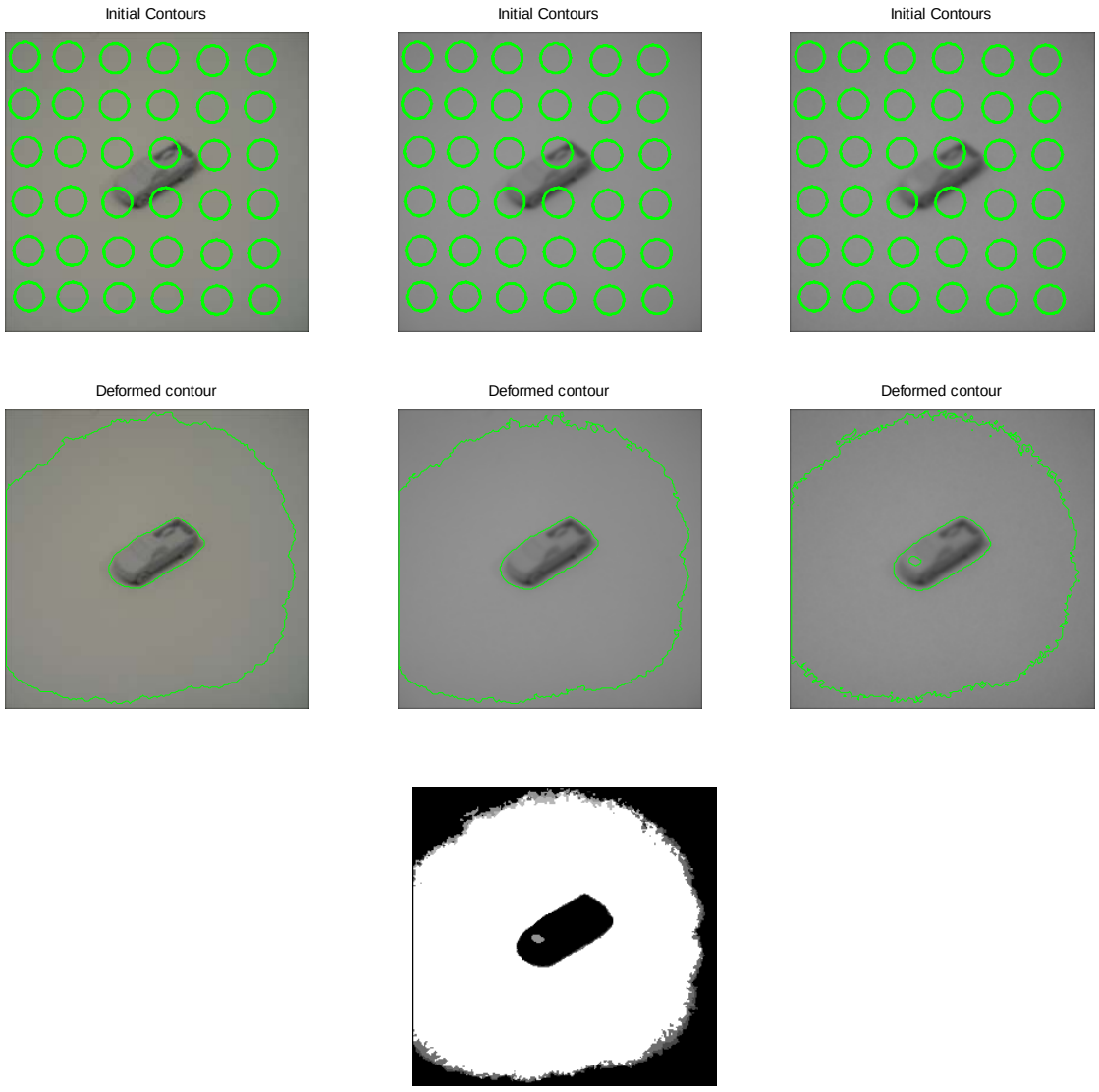

Figure 31 Proposed method applied into Figure 28 (7 bands). (Top) 2-phase Chan-Vese model applied separately into three groups. 36 initial contours are placed using distributed seeds in all three groups. (Middle) Active contours find only the silhouette of the car in the first two groups, but find the hot spot in the third group. (Bottom) The final result. The image is divided into eight segments (almost four segments by visual inspection) including the hot spot and the silhouette of the car.

How to define the number of group and which group each frame belongs to should be studied. As we increase the number of groups, we also increase the number of level set functions to calculate. The computational cost is as high as multi-phase active contours with one more dimension.

Conclusion and future works

We have done an investigation of active contours as an image segmentation method particularly for multispectral images. A research review on published methods has been performed with numerical experiments. Experimental results using selective models on various synthetic and real images are shown in this report. The segmented results have been evaluated using visual inspection.

The integration of the level set theory and the mean curvature motion into active contours allowed for automatic change of topology, such as merging and breaking, and the calculations are made on a fixed rectangular grid. The automatic topological changes make it possible to detect multiple objects, which is not possible for classical active contours. However, the level set function increased the dimension of data to update resulting in higher computational cost.

Depending on techniques used as stopping functions, we divided active contours into two groups; (a) geometry- or boundary-based models and (b) statistics- or region-based models. The boundary-based active contour models use the image gradient to stop the contour evolution on the desired boundary. Two boundary-based active contour models have been reviewed; geometric active contours and geodesic active contours. Although geometric active contours were not designed for vector-valued images, we could apply them into three-channel images using the average of the image gradient. The color snakes model was implemented as a particular example of geodesic active contours. The boundary-based active contours encounter a few limitations; (a) since the stopping function use the image gradient, boundary-based active contours make use of only local information like the classical snakes, and are sensitive to local minima and noise. (b) Due to the fact that the boundary-based active contours evolve an initial contour towards one direction, constrained by the curvature effect, the initial contour should be placed completely exterior or interior of the boundary of the object.

The region-based active contour models do not use the image gradient. Two region-based active contour models have been reviewed in this report; Chan-Vese model and Rousson-Deriche model. The region-based active contours show a few advantages compared to boundary-based active contours; (a) since region-based active contours do not need an edge function, objects without edge lines can be detected. Also, region-based active contours are more robust with respect to noise. (b) region-based stopping function is looking for the global (within the corresponding region) minimum instead of a local minimum. (c) The initial contour can be placed at anywhere in the image. The convergence speed can be improved by increasing the number of initial contours. (d) Multiple contours can be evolved

simultaneously providing multiple segments. According to visual inspection, region-based active contours often produce more reasonable segmentation.

Chan-Vese model uses Mumford-Shah segmentation techniques for the stopping function. Chan-Vese model represents the segmented image as a combination of constant vectors. Because of its simple structure, the contour evolution of Chan-Vese model is usually more than 5 times faster than Rousson-Deriche model, while Chan-Vese model is less applicable to complex images, particularly textured images. Rousson-Deriche model uses more general formulation obtained from the maximization of the *a posteriori* segmentation probability. Rousson-Deriche model represents the segmented image as a combination of multi-dimensional Gaussian distributions with adaptive mean vectors and covariance matrices. The contour evolution of Rousson-Deriche model is slower than Chan-Vese model, while Rousson-Deriche model is relatively more applicable to complex images because of the multi-dimensional (complex) structure.

We did an experiment of extracting a stack of prime active contours, which are evolved from a group of frames instead of the whole frames, in order to avoid the smoothing effect. This experiment showed that more discriminating features can be extracted from hyperspectral images.

After literature survey and numerical experiments, we have concluded that region-based active contours are more practical approaches than boundary-based active contours as a multispectral image segmentation tool. Active contours using multi-dimensional statistics, i.e. multi-dimensional histogram, are planed to study. We expect the multi-dimensional statistics to provide better segmentation ability with slightly higher computational cost. A supervised active contour model using histogram matching is also planned to study.

References

1. J. Canny, "a Computational Approach to Edge Detection," *IEEE Transactions on Pattern Analysis and Machine Intelligence*, no. 8, pp.769, 1986.
2. V. Caselles, F. Catte, T. Coll, F. Dibos, “a Geometric Model for Active Contours,” *Numerische Mathematik*, vol. 66, pp. 1, 1993.
3. V. Caselles, R. Kimmel, G. Sapiro, "Geodesic Active Contours," *International Conference on Computer Vision*, pp. 643, 1995.
4. V. Caselles, R. Kimmel, G. Sapiro, "Geodesic Active Contours," *International Journal of Computer Vision*, no. 1, pp. 61, 1997.
5. T. Chan, L. Vese, "Image Segmentation using Level Sets and the Piecewise-Constant Mumford-Shah Model," *UCLA Computational Applied Math Group Report*, no. 14, 2000.
6. T. Chan, L. Vese, "a Level Set Algorithm for Minimizing the Mumford-Shah Functional in Image Processing," *IEEE Workshop on Variational, Geometric and Level Set Methods in Computer Vision*, pp. 161, 2001.
7. T. Chan, Y. Sandberg, L. Vese, "Active Contours without Edges for Vector-Valued Images," *Journal of Visual Communication and Image Representation*, no. 11, pp. 130, 2000.
8. T. Chan, L. Vese, "Active Contours Without Edges," *IEEE Transactions on Image Processing*, no. 2, pp. 266, 2001.
9. L. Cohen, “on Active Contour Models and Balloons,” *Computer Vision Graphics Image Process: Image Understanding*, vol. 53, pp. 211, 1991.
10. L. Evans, R. Gariepy, *Measure Theory and Find Properties of Functions*, CRC press, 1992.
11. M. Kass, A. Witkin, D. Terzopoulos, "Snakes, Active Contour Model," *International Journal of Computer Vision*, pp. 321, 1988.
12. E. Kreyszig, *Differential Geometry*, University of Toronto Press, 1959.
13. R. Malladi, J. Sethian, “Image Processing via Level Set Curvature Flow,” *National Academy of Science*, vol. 92, pp. 7046, 1995.
14. R. Malladi, J. Sethian, C. Vemuri, "Shape Modeling with Front Propagation: a Level Set Approach," *IEEE Transactions on Pattern Analysis and Machine Intelligence*, no. 2, 1995.
15. D. Mumford, J, Shah, “Optimal Approximation by Piecewise Smooth Functions and Associated Variational Problems,” Communication Pure Applied Mathematics, vol. 42, pp. 577, 1989.
16. S. Osher, R. Fedkiw, “Level Set Methods: an Overview and Some Recent Results,” *Journal of computational Physics*, vol. 169, no. 2, pp. 463, 2001.
17. S. Osher, N. Paragios, *Geometric Level Set Methods in Imaging, Vision, and Graphics*, Springer,

2003.

18. S. Osher, J. Sethian, "Fronts Propagating with Curvature Dependent Speed: Algorithms Based on Hamilton-Jacobi Formulations," *Journal of Computationl Physics*, vol. 79, pp. 12, 1988.
19. N. Paragios, *Geodesic Active Regions and Level Set Methods*, PhD Thesis, INRIA, 2000.
20. N. Paragios, R. Deriche, "Geodesic Active Regions and Level Set Methods for Supervised Texture Segmentation," International Journal of Computer Vision, no. 3, pp. 223, 2002.
21. M. Rousson, R. Deriche, "a Variational Framework for Active and Adaptive Segmentation of Vector Valued Images," *IEEE Workshop on Motion and Video Computing*, 2003.
22. G. Sapiro, "Color Snakes," *Hewlett-Packard Labs Report*, no. 113, 1995.
23. G. Sapiro, "Color Snakes," *Computer Vision and Image Understanding*, no. 2, pp. 247, 1997.
24. J. Sethian, *Level Set Methods*, Cambridge University Press, 1996.
25. L. Vese, T. Chan, "A Multiphase Level Set Framework for Image Segmentation Using the Mumford and Shah Model," *International Journal of Computer Vision*, no. 3, pp. 271, 2002.
26. C. Xu, A. Yezzi, J. Prince, "a Summary of Geometric Level Set Analogues for a General Class of Parametric Active Contour and Surface Models," *IEEE Workshop on Variational, Geometric and Level Set Methods in Computer Vision*, pp 104, 2001.